The electric behavior of a lithium-niobate-phosphate glass and glass-ceramics

M. P. F. GRAÇA, M. A. VALENTE
Departamento de Física, Universidade de Aveiro, 3800-193 Aveiro, Portugal

M. G. FERREIRA DA SILVA
Departamento de Engenharia Cerâmica e do Vidro (CICECO), Universidade de Aveiro, 3800-193 Aveiro, Portugal

Published online: 4 February 2006

A glass with a composition of $50Li_2O$-$40P_2O_5$-$10Nb_2O_5$ (% mol) was prepared by the melt-quenching method and heat-treated in air between 450 and 500°C. The samples were studied using X-ray powder diffraction (XRD), density measurements, Raman spectroscopy, scanning electron microscopy (SEM), dc electrical conductivity (σ_{dc}) and dielectric measurements.

The $LiNbO_3$ crystalline phase was detected in the samples heat-treated at 480 and 500°C. The dc conductivity, at 300 K, decreases and the activation energy increases with the rise of the heat-treatment temperature. The dielectric data between 1 Hz and 100 kHz, at room temperature, were studied using the impedance formalism (Z^*). These results show the existence of a relaxation mechanism, probably associated with a distribution of relaxation times. The mean value of the relaxation time, τ_σ, increases with the rise of the heat-treatment temperature. The fit of the dielectric data with a complex nonlinear least squares algorithm (CNLLS), reveals that a resistor (R), in parallel with a constant phase element (CPE, $Z_{CPE} = 1/[Y_0(jw)^n]$), is a good equivalent circuit. The R-value has a maximum for the sample heat-treated at 480°C, and the n parameter has the inverse behavior. The Y_0 parameter decreases with the increase of the heat-treatment temperature.

The dielectric constant value, at 1 kHz and room temperature, increases from 39.98 up to 97.80 with the rise of the heat-treatment temperature. These results suggest that exists a relation between the number of $LiNbO_3$ ferroelectric crystals present in the glass-ceramics and the dielectric constant values.

1. Introduction

In recent years there has been a considerable amount of interest in the preparation, and study of the physical properties, of glass-ceramics with ferroelectric crystalline phases [1]. An important ferroelectric material is lithium niobate, $LiNbO_3$, due to its excellent pyroelectrical, piezoelectrical and photorefractive properties [2–4]. This material has a high Curie temperature, $T_c = 1210$°C [3, 5]. However, the usual preparation of $LiNbO_3$ crystals, by the Czochralski method, is time consuming, very expensive and with Li deficiency crystals [1, 2, 6]. Glass-ceramics, with the ferroelectric crystal phase, seems to be an interesting alternative due to its relative low preparation time and costs.

The purpose of the present study is to prepare glass-ceramics containing $LiNbO_3$ crystals. An attempt has been made to establish a correlation between the electrical properties of the glass and glass-ceramics and their microstructure.

2. Experimental procedures

A glass with the composition $50Li_2O$-$40P_2O_5$-$10Nb_2O_5$ (mol%) was prepared using the melt-quenching method. The glass was prepared from the reagent grade lithium carbonate (Li_2CO_3 - Merck), ammonium dihydrogen phosphate ($NH_4H_2PO_4$ - Merck) and niobium oxide

0022-2461
DOI: 10.1007/s10853-005-3652-6

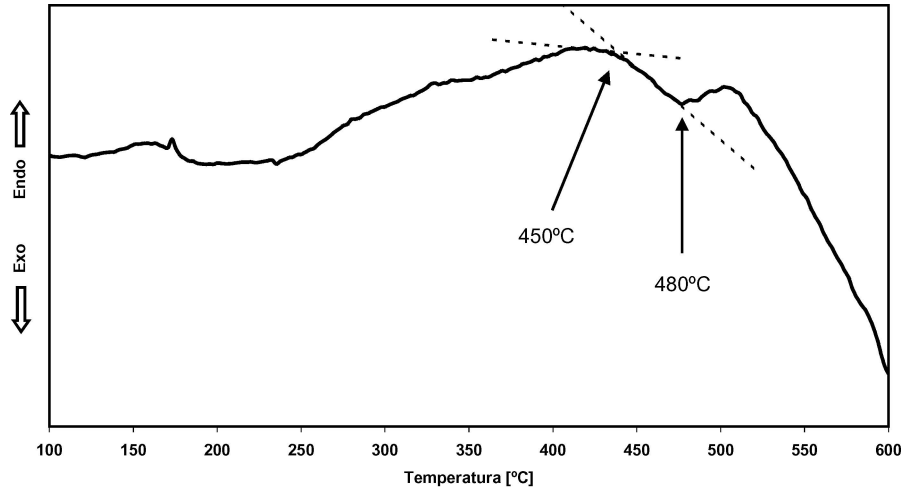

Figure 1 DTA spectra of the $50Li_2O$-$40P_2O_5$-$10Nb_2O_5$ glass composition.

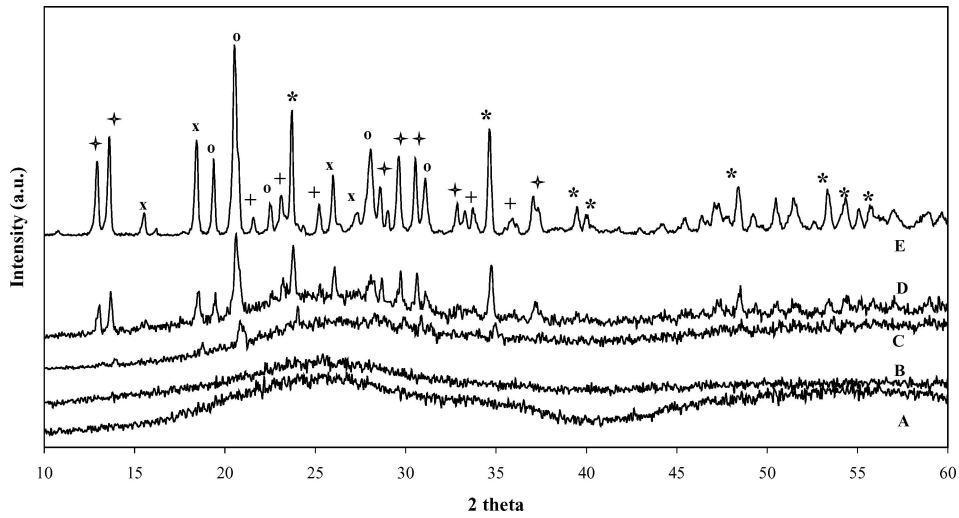

Figure 2 XRD spectra of the A, B, C, D and E samples (+ Li_3PO_4; x $LiPO_3$; o $Li_4P_2O_7$; ∗ $LiNbO_3$; ✦ unidentified phase [20]).

(Nb_2O_5 –Merck). The reagents, in appropriate amounts, were mixed for 1 h, in an agate ball-mixing planetary system. The mixture was heated in a platinum crucible at 700°C, for approximately 48 hours, to remove the CO_2 from the Li_2CO_3, and water and ammonia from $NH_4H_2PO_4$, and then melted at 1200°C for 1 h. The melt was poured into a stainless steel mould pre-heated at 300°C. The result was a yellow and transparent glass (sample A).

Glass samples with a thickness of approximately 10^{-3} m were heat-treated in air, with a heating rate of 75°C/h, at 450°C (B sample), at 480°C (C sample) and at 500°C (E sample) during 4 h and at 500°C during 2 h (D sample). These temperatures were chosen in agreement with the differential thermal analysis results (DTA), carried out with a *Linseis* apparatus, starting at room temperature until 1100°C, with an heating rate of 5°C/min (Fig. 1).

The X-ray diffraction patterns (XRD) were obtained at room temperature, using powdered samples, in a *Philips X'Pert* system, with a K_α radiation (λ=1.54056 Å) at 40 kV, and 30 mA, with a step of 0.05° and a time per step of 1 s (Fig. 2).

The density measurements were realized in a Adam Equipment ADP-110 system, measuring the sample weight in air and in C_2H_5OH, at 300 K (Archimedes principle).

The Raman spectroscopy was carried out in a T64000, Jobin Yvon SPEX spectrometer using an Ar laser (λ=514.5 nm). The spectra were obtained, in a back-scattering geometry, between 100 and 2000 cm^{-1} (Fig. 3).

The microstructure of the glass and glass-ceramics was observed by scanning electron microscopy (SEM), performed in a *Hitachi S4100-1* system, on the surface and fracture surface of all samples covered with carbon before microscopic observation (Fig. 4).

For the electrical measurements, aluminum electrodes were sputtered on the opposite sides of disc shaped

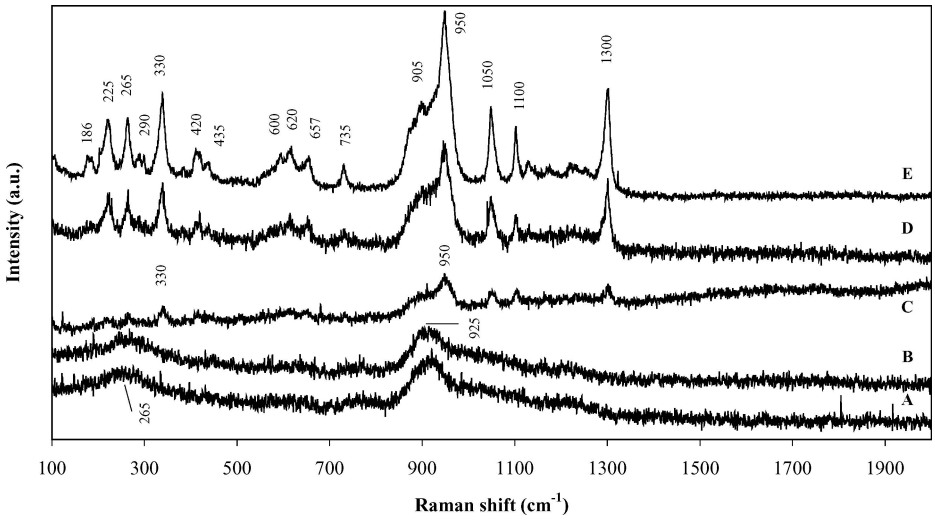

Figure 3 Raman spectra of the A, B, C, D and E samples.

samples, with 5×10^{-3} m of diameter. During the electrical measurements the samples, with a thickness about 10^{-3} m, were in a helium atmosphere, to improve the heat transfer and eliminate the moisture.

The impedance spectroscopy measurements were carried out at room temperature, in the frequency range of 1 Hz-100 kHz using a *SR850 DSP Lock-In Amplifier*, in the typical lock-in configuration, measuring the "in-phase" and "quadrature" components of the output signal [7].

The analytical background, used in the electrical data analysis, was as follows:

(a) The *Arrhenius* expression [8] has been used to fit the temperature dependence of the dc conductivity, σ_{dc} (Equation 1):

$$\sigma_{dc} = \sigma_0 \exp\left(-\frac{E_{a(dc)}}{k_B T}\right) \tag{1}$$

where σ_0 is a pre-exponential factor, $E_{a(dc)}$ the activation energy, k_B the Boltzmann constant and T the temperature.

(b) The complex permittivity, $\varepsilon^* = \varepsilon' + j\varepsilon''$, was interpreted using the complex impedance formalism, $Z^* = 1/(\mu\varepsilon^*)$ [9, 10] (where $\mu = j\omega C_0$, ω is the angular frequency, C_0 the admittance of the empty cell and $j = \sqrt{-1}$ [11]). The real and imaginary parts of the impedance were calculated using Equation 2.

$$Z^* = \frac{R_i\left(V_f V_0 - V_f^2 - V_q^2\right) - \omega C_i^2 R_i^2 V_q V_0}{\left(1+\omega^2 C_i^2 R_i^2\right)\left(V_f^2 + V_q^2\right)} - j\frac{V_q V_0 R_i + \omega C_i^2 R_i^2\left(V_f V_0 - V_f^2 - V_q^2\right)}{\left(1+\omega^2 C_i^2 R_i^2\right)\left(V_f^2 + V_q^2\right)} \tag{2}$$

This expression was obtained when the sample impedance is in series with a known resistance (1 kΩ). This resistance is in parallel with the lock-in input impedance. R_i is the equivalent resistance of the lock-in input resistance (100 MΩ) and the known resistance (1 kΩ), C_i the lock-in input capacitance (15 pF), V_0 the input signal ($|V_0|$=1 V), and V_f and V_q the phase and quadrature components of the measured signal.

A quantitative characterization of the dielectric measurements was made using a complex nonlinear least squares (CNLLS) algorithm associated with the Levenberg-Marquardt method [12–14]. This software was developed with the main aim of fitting the frequency dependent impedance data with the values calculated from an equivalent circuit [14], characterized by a resistance (R) in parallel with a constant phase element (CPE) [9, 10]. The impedance of this intuitive element can be defined by $1/Z_{CPE} = Y_0(j\omega)^n$ where Y_0 ($[Y_0]$=Fs^{n-1}) is the admittance (Y_0=$1/|Z^*|$) at $\omega = 1$ rad/s and n a value between 0 and 1. The Y_0 and n parameters are independent of the frequency. When $n = 1$, Z_{CPE} is an ideal capacitive element [9]. The developed algorithm calculates the R, Y_0 and n parameters that best fit the measured data.

The complex modulus formalism (M^*=$1/\varepsilon^*$), proposed by Macedo [15], was adopted to determine the relaxation time (τ_σ), because it minimizes the electrode interface capacitance contribution and others interfacial effects [11, 15]. The representation of M″ versus frequency (in logarithmic scale) often shows peak(s) associated with the contribution(s) of small capacitance(s) [15, 16]. The relaxation time is defined by τ_σ=$(\omega_{peak})^{-1}$, where ω_{peak}

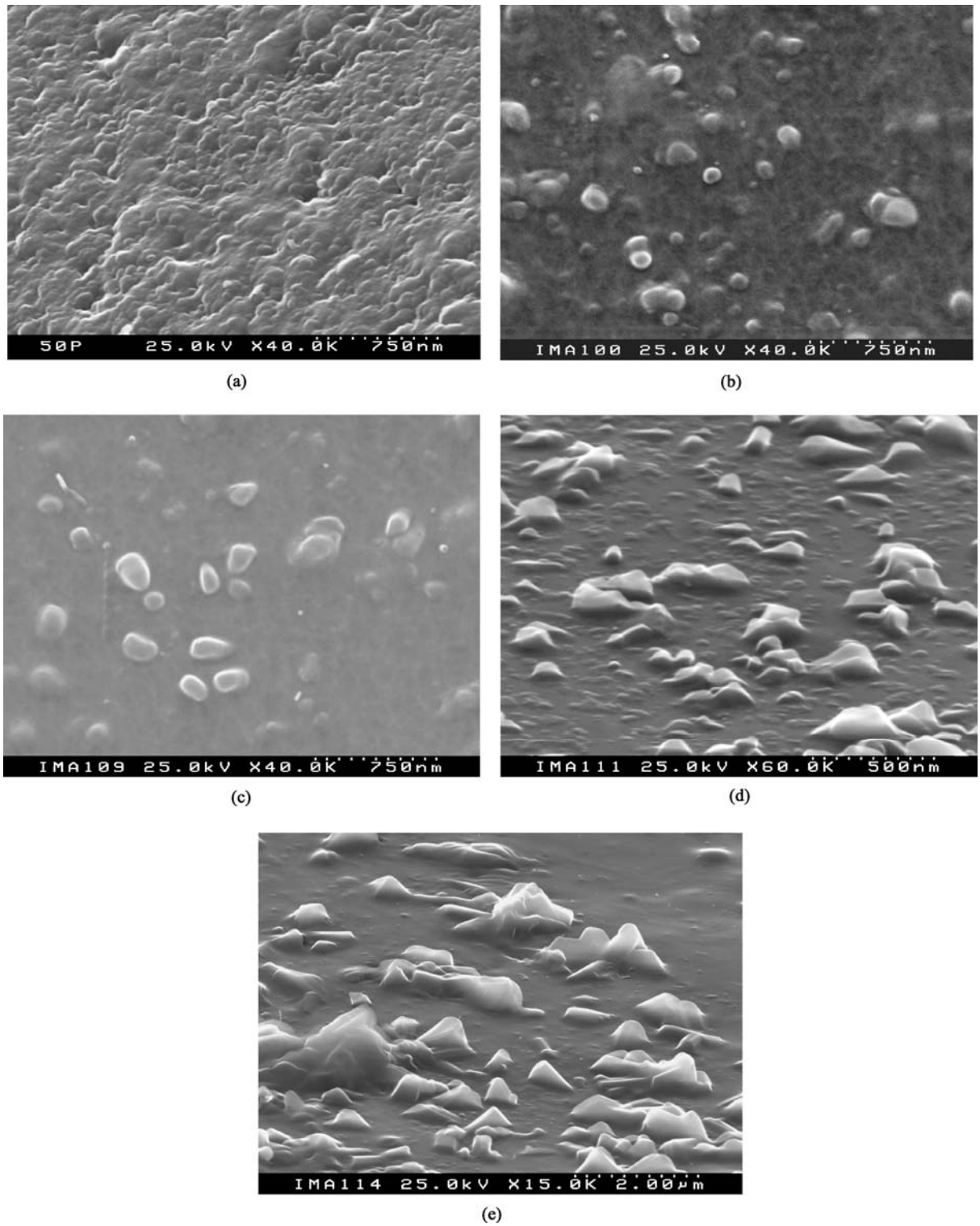

Figure 4 SEM micrograph of the A(4.a), B(4.b), C(4.c), D(4.d) and E(4.e) fracture surface samples.

represents the angular frequency of the M″ peak(s) [9, 17].

3. Results

The differential thermal analysis of the as-prepared sample (sample A) shows that the glass transition temperature is approximately 450°C (Fig. 1). The sample heat-treatment temperatures were chosen in agreement with this value (Table I).

In the A and B samples the presence of crystalline phases was not detected by XRD (Fig. 2). However, in the C, D and E samples are present the $LiNbO_3$, Li_3PO_4, $Li_4P_2O_7$ and $LiPO_3$ crystalline phases [18].

TABLE I The heat-treatment (HT) conditions, the dc conductivity (σ_{dc}) measured at 300 K, the dc activation energy ($E_{a(dc)}$), the dielectric constant (ε') measured at 1 kHz and room temperature, the relaxation time (τ_σ) and the density (ρ). In parenthesis are the correspondent statistic errors

Sample	HT conditions (temperature — °C/time –h)	ρ (g/cm^3)	σ_{dc} ($\times 10^{-6}$) $(\Omega m)^{-1}$ (300 K)	σ_0 ($\times 10^3$) $(\Omega m)^{-1}$	$E_{a(dc)}$ (kJ/mol)	ε' (300 K, 1 kHz)	τ_σ ($\times 10^{-6}$) (s)
A	as-prepared	2.698 (±0.008)	9.35 (±1.09%)	58.32 (±0.25)	56.0 (±0.56)	39.98 (±1.13)	5.52
B	450°C/4 h	2.728 (±0.041)	8.56 (±1.04%)	30.73 (±0.18)	55.1 (±0.41)	40.65 (±1.36)	7.39
C	480°C/4 h	2.811 (±0.051)	3.39 (±1.40%)	9.46 (±0.16)	60.1 (±0.31)	79.48 (±2.51)	7.67
D	500°C/2 h	2.679 (±0.064)	3.01 (±1.37)	64.89 (±0.35)	65.9 (±0.81)	94.69 (±2.76)	7.97
E	500°C/4 h	2.729 (±0.038)	2.90 (±1.32%)	75.23 (±0.28)	65.7 (±0.63)	97.80 (±3.09)	8.61

The density of the glass and glass-ceramics (Table I) shows a maximum for the C sample (2.811 g/cm^3).

Fig. 3 shows the Raman spectra of all the samples. The broad bands at 925 and 265 cm^{-1}, observed in the A and B samples, are attributed to the P-O bending and to the vibration of NbO_6 units, respectively [19–21]. The bands at 620, 420, 330, 265 and 225 cm^{-1}, observed in the C, D and E samples, the band at 620 cm^{-1} observed in the D and E samples, and the bands at 950, 600, 435 and 290 cm^{-1} observed in the E sample reveal the presence of NbO_6 octahedron [2, 11, 20–23c]. In the Raman spectra of the referred samples, the bands at 1300, 1100, 1050, 950 and 735 cm^{-1} are associated to the P-O vibrations [23–28]. The band at 1100 cm^{-1} is assigned to the $LiPO_3$ chain type, the band at 1050 cm^{-1} is attributed to the presence of pyrophosphate $Li_4P_2O_7$ crystals, and the 950 cm^{-1} peak, that it is the most intense in the C, D and E samples, is associated to the orthophosphate Li_3PO_4 crystalline phase [21]. In the D and E samples, the band at 225 cm^{-1} may be attributed to NbO_6 vibrations [20]. In the E sample, the band at 186 cm^{-1} is ascribed to the P-O-P bend [29] and the bands at 905 and 657 cm^{-1}, are assigned to the Nb^{5+} ions incorporated in the phosphate glass structure (in octahedral coordination) [20].

The SEM results show that the A sample does not have particles. In the B sample surface the presence of particles was detected (Fig. 4). The size of these particles increases, with the rise of the heat-treatment temperature and their number decrease from the D to the E samples (Fig. 4).

The dc conductivity (σ_{dc}), at room temperature (300 K), decreases from the A sample (9.35×10^{-7} Ω^{-1} m^{-1}) to the E sample ($2.90 \times 10^{-7} \Omega^{-1}m^{-1}$) (Table I). The activation energy ($E_{a(dc)}$), of this conductivity process was determined from the slope of $\ln(\sigma_{dc})$ versus $1/T$ (Fig. 5.) (Equation 1) and it increases from 56.0 to 65.7 kJ/mol (Table I) from the A to the E samples.

Fig. 6 shows the impedance spectra, Z′ versus Z″, of all samples. In this figure the points represent the experimental data (1 Hz<f<100 kHz) and the line the theoretical fit (4 kHz<f<100 kHz). The centers of the semicircles are below the Z′ axes. From the analysis of the CNLLS fit values (Table II) it can be verified that, with the increase of the heat-treatment temperature: the R value increases, from 3.24 MΩ to 19.7 MΩ; the Y_0 value decreases from 1.20×10^{-10} to 6.04×10^{-11}; the n parameter decreases from 0.84 (A sample) to 0.77 (C sample) and then increases to 0.81 (E sample). In the impedance spectra, Z′ versus Z″, for the C, D and E samples is present a Warburg response type [9] at low frequencies (Fig. 6), that limits the frequency range used in the theoretical fits.

It was found that ε', measured at 1 kHz and room temperature, increases from 39.98 to 97.80, with the increase of the heat-treatment temperature of the samples (Table I).

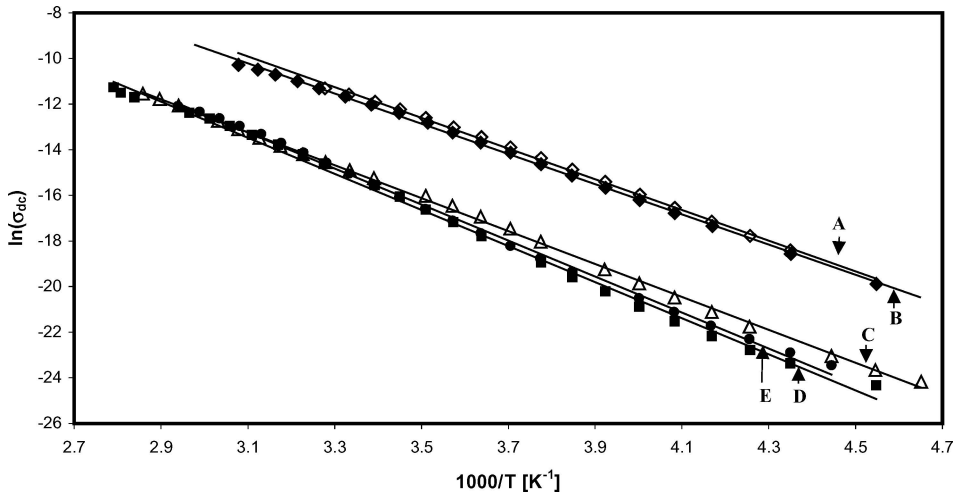

Figure 5 $\ln(\sigma_{dc})$ vs $1000/T$ spectra of the A(◊), B(♦), C(△), D(■) and E(●) samples.

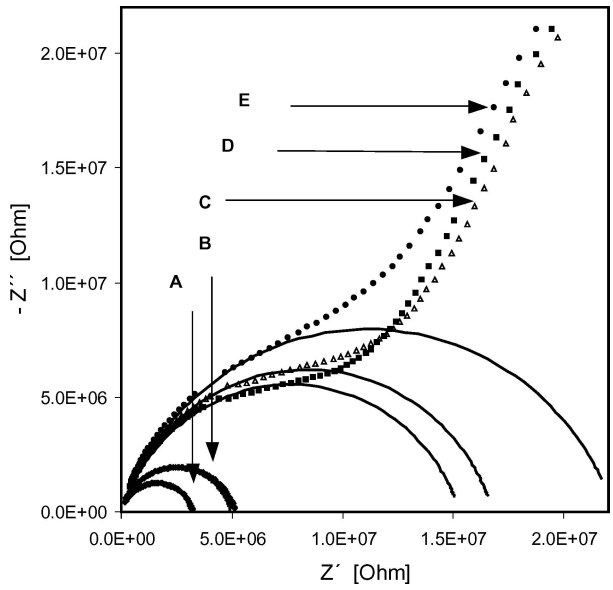

Figure 6 Z′ vs Z″ spectra of the A(◇), B(♦), C(△), D(■) and E(●) samples (the points are the experimental data and the lines the theoretical fit).

Fig. 7 represents the frequency distribution of M″ data, showing a maximum for all the samples. It is known that M'' has a maximum when $\omega\tau_\sigma = 1$. τ_σ represents the mean value of the relaxation time distribution observed with the modulus formalism [9, 17]. In these samples this maximum shifts to lower frequencies (Table I), with the increase of the heat-treatment temperature.

4. Discussion

The niobium silicate samples heat-treated above 480°C (C, D and E samples) suffer crystallization. Thus, the XRD patterns show the formation of the $LiNbO_3$, Li_3PO_4, $Li_4P_2O_7$ and $LiPO_3$ crystalline phases and the width of the Raman bands decreases [19] with the rise of the heat-treatment temperature. The presence of octahedral coordinated Nb^{5+} ions, in the samples, promotes the formation of $LiNbO_3$ crystallites. However, the obtained glass-ceramics has, also, others crystalline phases (Li_3PO_4, $Li_4P_2O_7$ and $LiPO_3$). On the contrary in the glass ceramics obtained from the glass with the composition $34SiO_2$ $33Li_2O$-$33Nb_2O_5$ (% mol) we have only the $LiNbO_3$ phase [30]. In the B sample (heat-treated at 450°C), it is not detected the presence of crystalline phases, neither in the XRD pattern nor in the Raman spectrum (Figs 2 and 3.). Nevertheless, SEM micrograph shows the presence of particles (Fig. 4) and ε' increases from A to B samples (Table I). This increase in ε' indicates an increase in the dipole moment. Also, the τ_σ values increases from A to B samples (Table I) indicating a higher difficulty of depolarization in the B sample ($LiNbO_3$ crystals are hard to depolarize [3, 4]). Thus, it may be reasonable to assume that, in the B sample, $LiNbO_3$ crystals are present.

In the C, D and E samples there is an increase in the ε' and τ_σ values because the fraction of lithium niobate, present in the glass matrix, increases. However, the maximum value obtained, for ε', was 99 (E sample- Table I) and the $LiNbO_3$ single crystal presents a ε' higher than 1000, at 1 kHz and 300 K [31–33]. This difference in the ε' value is due, in our opinion, to the fact that the $LiNbO_3$ crystallites are inserted in a glass matrix and are not oriented in a preferential direction.

When comparing the results obtained by Graça *et al.* [30], in a silicate glass system, and the results obtained in this work it seems that the growth in a preferential direction, of the $LiNbO_3$ crystals, is easier in the phosphate glasses. This phenomenon can be ascribed to the structural characteristics of the phosphate glass network, which is remarkably different from that of the silicate glasses, due to the presence of terminal oxygen atoms (oxygen atoms double bonded to the P^{5+} ion, in the basic PO_4 structure), that makes the phosphate glasses a good environment for the cations accommodation. According to Hoppe *et al.* [34] in binary phosphate glasses, where the quantity of network modifiers is above 20% mol, there are not enough individual terminal oxygen atoms to satisfy the coordination environments of every cation and these ions must share the available terminal oxygen. This structural arrangement leads to the formation of non-uniform electric charge-zones distribution. These non-uniform charge-zones can create an internal electric field that makes favorable the growing of the crystals in a preferential direction.

The dc measurements reveal a decrease in the σ_{dc} values (Table I), from the A to the E sample, justified with the decrease on the Li^+ ions present in the glass matrix. Thus, with the increase of the heat-treatment temperature, the Li^+ ions are inserted in crystalline structures (see XRD – Fig. 2). The behavior of the $E_{a(dc)}$ (Table I) can also be associated with the decrease in the Li^+ ions inside the glass matrix and suggests an increasing in the height of the free energy barriers of the quasi-lattice of the glass matrix with the increase of the heat-treatment temperature [8, 11, 17].

TABLE II The equivalent circuit characteristics (from the CNLLS fit procedure) and the statistic errors, for all the samples

Sample	R ($\times 10^6$)	ΔR	Yo ($\times 10^{-11}$)	ΔYo	n	Δn
A	3.24	(<1%)	12.0	(<1%)	0.842	(<1%)
B	5.16	(<1%)	10.4	(<1 %)	0.837	(<1%)
C	18.2	(±2.5%)	9.46	(±1.49%)	0.776	(<1%)
D	14.4	(±1.75%)	7.67	(±1.42%)	0.806	(<1%)
E	19.7	(±2.72%)	6.04	(±2.18%)	0.816	(<1%)

4.1. Analysis of the impedance data

From the Z′ versus Z″ plot (Fig. 6), it can be observed that the semi-arcs, which centers are under the Z′ axes, indicate the existence of a distribution (dispersion) of relaxation times [9, 10, 17, 32] that should be associated to the fact that in this system, the ferroelectric phase is embedded in the glass matrix. In the C, D and E samples a low-frequency Warburg response type [9] is observed, and can be attributed to the relaxation of the sample/electrode

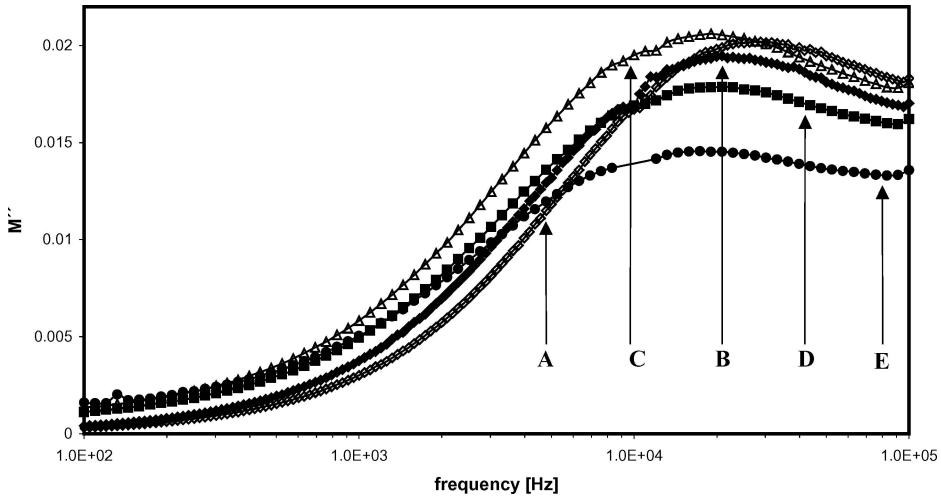

Figure 7 M″ vs frequency spectra of the A(◇), B(♦), C(△), D(■) and E(●) samples.

interface dipoles. The theoretical fit of these data (Fig. 6) shows that a resistance in parallel with a CPE element is an equivalent circuit that describes the measured data. However, it was not easy to find a total supported correlation between the calculated theoretical values (Table II) and the samples characteristics. Nevertheless, the increase on the R parameter can be related to the increase in the amount of the $LiNbO_3$ crystallites. The decrease on the R parameter, from C to the D sample, can be justified by the increase on the amount of the lithium phosphate crystals (Li_3PO_4, $Li_4P_2O_7$ and $LiPO_3$). In the D sample, the number of those crystals, in which resistivity is lower than that of $LiNbO_3$, should be higher than in the C sample. This assumption is supported by the XRD spectra (Fig. 2), where it can be seen an increase in the number, and sharpness, of the peaks associated with the lithium phosphate phases. On the other hand the $LiNbO_3$ crystals have a higher density than the lithium phosphate crystallites [23] and it is observed a decrease in the density from the C to the D samples (Table I). Thus, it may be assumed that the behavior of the R parameter can be associated with the number of $LiNbO_3$ and the lithium phosphate crystallites present in the glass matrix.

From the A to the C sample, the obtained n values (Table II), associated with the Kohlrausch exponent (β) by the expression $\beta=1-n$ [35], are in agreement with that obtained for the Li_2O-P_2O_5 binary glasses [11]. In the Li_2O-P_2O_5 binary glasses the β value decreases with the increase of the alkali ion content [11]. However, in the D and E samples, the amount of Li^+ ions present in the glass matrix decreases with the rise of the heat-treatment temperature, but the β value decreases. Thus, the β behavior of the phosphate glass is strongly dependent on the presence of niobium and crystalline phases.

5. Conclusions

The molar composition $50Li_2O$-$40P_2O_5$-$10Nb_2O_5$ gives origin to a transparent and yellow glass. This composition does not promote the preparation of glass-ceramics with only $LiNbO_3$ crystallites because in the samples are also present the Li_3PO_4, $Li_4P_2O_7$ and $LiPO_3$ crystalline phases.

The electrical results suggest a decrease on the number of Li^+ ions in the glass matrix, with the increase of the heat-treatment temperature, and an increase in the volume fraction of $LiNbO_3$ ferroelectric crystallites (the dielectric constant increases with the increasing of the heat-treatment temperature). The existence, in all the samples, of a semi-arc in the Z′ versus Z″ plot, which center is under the Z′ axis, indicates the existence of a relaxation time distribution. The mean value of this relaxation distribution, τ_σ, increases, with the rise of the heat treatment temperature, and should be associated with the increase in the amount of $LiNbO_3$ ferroelectric crystalline phase, whose dipoles are difficult to depolarize at room temperature. The CNLLS fit results show that a resistor in parallel with a CPE element is a good equivalent circuit.

In comparison with the SiO_2–Li_2O-Nb_2O_5 glass system [30] the P_2O_5-Li_2O-Nb_2O_5 glass is disadvantageous because it is not possible to obtain glass-ceramics containing $LiNbO_3$ crystals alone. In both systems, the dc conductivity is high ($\sigma_{dc}>10^{-7}$ Ω^{-1} m^{-1}, at 300 K), and decreases with the increase of the heat-treatment temperature. This behavior is due to the increase of the amount of $LiNbO_3$ crystallites with the rise of the heat-treatment temperature and a decrease in the Li^+ ions present in the glass matrix. However, the growth of $LiNbO_3$ crystallites with a preferential orientation seems to be easier in the P_2O_5 glass system than in silicate glasses.

Acknowledgements

The authors thank to the Fundação para a Ciência e Tecnologia (FCT), for the financial support (SFRH/ BD/ 6314/ 2001).

References

1. T. KOMATSU, H. TAWARAYAMA, H. MOHRIN and K. MATUSITA, *J. Non-Cryst. Solids* **135** (1991) 105.
2. S. HIRANO, T. YOGO, K. KIKUTA and Y. ISOBE, *J. Mater. Sci.* **28** (1993) 4188.
3. M. M. ABOULLEIL and F. J. LEONBERGER, *J. Am. Ceram. Society* **72** (1989) 1311.
4. E. M. VOGEL, *ibid.* **72** (1989) 719.
5. E. B. DE ARAUJO, J. A. C. DE PAIVA, M. A. B. DE ARAUJO and A. SERGIO BEZERRA SOMBRA, *Physica Scripta.* **53** (1996) 104.
6. H. G. KIM, T. KOMATSU, R. SATO and K. MATUSITA, *J. Non-Cryst. Solids* **162** (1994) 201.
7. SR850, DSP Lock-In Amplifier Operating Manual and Programming Reference, Standford Research Systems, California, USA, 1992.
8. S. W. MARTIN and C. A. ANGELL, *J. Non-Cryst. Solids* **83** (1986) 185.
9. J. R. MACDONALD, *Impedance spectroscopy*, (John Wiley & Sons, New York, 1987).
10. A. K. JONSCHER, (*Dielectric relaxation in solids*), Chelsea Dielectrics Press, London, 1983.
11. B. V. R. CHOWDARI and K. RADHAKRISHNAN, *J. Non-Cryst. Solids* **110** (1989) 101.
12. P. R. BEVINGTON, *Data Reduction and Error Analysis for the Physical Sciences*, (McGraw-Hill, EUA, 1969).
13. B. A. BOUKAMP, *Solid State Ionics* **11** (1984) 339; B.A. Boukamp, *Solid State Ionics,* 20 (1986) 31.
14. M. P. F. GRAÇA, M. A. VALENTE and M. G. F. SILVA, to be published.
15. P. B. MACEDO, C. T. MOYNIHAN and R. BOSE, *Phys. Chem. Glasses* **13**(6) (1972) 171.
16. J. C. C. ABRANTES, J.A LABRINCHA and J. R. FRADE, *Mat. Res. Bull.* **35** (2000) 727.
17. KIA LA. NGAI and RONALD W. RENDELL in "*Handbook of conducting polymers*", vol II, Marcel Dekker, NY, 1986.
18. JCPDS data base.
19. V. C. FARMER, "*The infrared spectra of minerals*", Mineralogical Society, London, 1974.
20. J. S. ANDRADE, A. G. PINHEIRO, I. F. VASCONCELOS, J. M. SASAKI, J.A.C. PAIVA, M. A. VALENTE and A.S.B. SOMBRA, *J. Phys. Cond. Matter* **11** (1999) 4451.
21. M. TATSUMISAGO, Y. KOWADA and T. MINAMI, *Phys. Chem. of Glasses* **29**(2) (1988) 63.
22. K. FUKUMI and S. SAKKA, *J. Mater. Sci.* **23** (1988) 2819.
23. (a) Merck Chemical database (www.chemdat.de); (b) Alfa Aesar database (www.alfa.com); (c) Aldrich database (www.aldrich.com).
24. F. L. GALEENER and J. C. MIKKELSEN, Jr., *Solid State Communications* **30** (1979) 505.
25. K. J. RAO, K. C. SOBHA and S. KUMAR, *Proc. Indian. Acad. Sci. (Chem. Sci.)* **113** (5–6) (2001) 497.
26. M. SCAGLIOTTI, M. VILLA and G. CHIODELLI, *J. Non-Cryst. Solids* **93** (1987) 350.
27. N. SHIBATA, M. HORIGUDHI and T. EDAHINO, *ibid.* **45** (1981) 115.
28. A. MOGUS-MILANKOVIC and D. E. DAY, *ibid.* **162** (1993) 275.
29. J. J. HUDGENS, R. K. BROW, D. R. TALLART and S. W. MARTIN, *ibid.* **223** (1998) 21.
30. M. P. F. GRAÇA, M. A. VALENTE and M. G. F. SILVA, *ibid.* **325**(1–3) (2003) 267.
31. M. V. SHANKAR and K.B.R. VARMA, *ibid.* **243** (1999) 192.
32. M. M. EL-DESOKY, S. M. SALEM and I. KASHIF, *J. Mat. Sci* **10** (1999) 279.
33. M. TODOROVIC and L. RADONJIC, *Ceramics International* 23 (1997) 55.
34. U. HOPPE, G. WALTER, R. KRANOLD and D. STACHEL, *J. Non-Cryst. Solids* **263&264** (2000) 29.
35. K. L. NGAI and S. W. MARTIN, *Physical Review B* **40**(15) (1989) 10550.

Received 26 May 2004
and accepted 9 May 2005